CORE
Metadata, citation and similar papers at core.ac.uk
Provided by Repositório Científico do Instituto Politécnico do Porto

PHYSICAL REVIEW B **84**, 024120 (2011)

Photoluminescence and electrical study of fluctuating potentials in Cu_2ZnSnS_4-based thin films

J. P. Leitão,[1,*] N. M. Santos,[1] P. A. Fernandes,[1,2] P. M. P. Salomé,[1] A. F. da Cunha,[1] J. C. González,[3] G. M. Ribeiro,[3] and F. M. Matinaga[3]

[1]*Departamento de Física, Instituto de Nanoestruturas, Nanomodelação e Nanofabricação, Universidade de Aveiro, Campus Universitário de Santiago, P-3810-193 Aveiro, Portugal*

[2]*Departamento de Física, Instituto Superior de Engenharia do Porto, Instituto Politécnico do Porto, Rua Dr. António Bernardino de Almeida, 431, P-4200-072 Porto, Portugal*

[3]*Departamento de Física, Universidade Federal de Minas Gerais, 30123-970 Belo Horizonte, Minas Gerais, Brazil*

(Received 31 August 2010; published 29 July 2011)

In this work, we investigated structural, morphological, electrical, and optical properties from a set of Cu_2ZnSnS_4 thin films grown by sulfurization of metallic precursors deposited on soda lime glass substrates coated with or without molybdenum. X-ray diffraction and Raman spectroscopy measurements revealed the formation of single-phase Cu_2ZnSnS_4 thin films. A good crystallinity and grain compactness of the film was found by scanning electron microscopy. The grown films are poor in copper and rich in zinc, which is a composition close to that of the Cu_2ZnSnS_4 solar cells with best reported efficiency. Electrical conductivity and Hall effect measurements showed a high doping level and a strong compensation. The temperature dependence of the free hole concentration showed that the films are nondegenerate. Photoluminescence spectroscopy showed an asymmetric broadband emission. The experimental behavior with increasing excitation power or temperature cannot be explained by donor-acceptor pair transitions. A model of radiative recombination of an electron with a hole bound to an acceptor level, broadened by potential fluctuations of the valence-band edge, was proposed. An ionization energy for the acceptor level in the range 29–40 meV was estimated, and a value of 172 ± 2 meV was obtained for the potential fluctuation in the valence-band edge.

DOI: 10.1103/PhysRevB.84.024120 PACS number(s): 78.20.−e, 68.55.−a, 68.37.Hk, 73.50.Jt

I. INTRODUCTION

The solar cell market is dominated by cells based on silicon wafers. However, due to the high materials costs and new concepts such as building-integrated architecture, other technologies have been implemented, some of these being the "second generation" thin-film approaches based on different materials.[1] The one with the best reported performance is $CuIn_{1-x}Ga_xSe_2$ (CIGS), for which efficiencies of 20.3% have been measured in the laboratory.[2] However, due to the low availability of In and Ga in the Earth's crust, the increasing world demand for ITO touch-sensitive displays, and the toxicity of Se, Cu_2ZnSnS_4 (CZTS) in the kesterite phase has been proposed as a candidate to replace CIGS as the cell absorber layer. CZTS has an absorption coefficient over 10^4 cm^{-1} and a band gap of ~ 1.5 eV,[3–8] which makes it suitable for applications in thin-film solar cells. The deposition of the precursors can be done under vacuum conditions as in the case of electron-beam evaporation[3,9,10] or radiofrequency (rf) magnetron sputtering.[4,11] Alternatively, the deposition of the precursors can be done under nonvacuum conditions as, for example, through spray pyrolysis,[12,13] the sol-gel method,[5] or sol-gel spin-coated deposition.[14] The CZTS is formed with a subsequent sulfurization of the precursors. In a different approach, Friedlmeier *et al.*[15] deposited CZTS films using thermal co-evaporation. The highest attained efficiency for CZTS-based solar cells was 6.8%,[16] whereas for $Cu_2ZnSn(S,Se)_4$-based solar cells it was 9.6%.[17] To improve the efficiency of solar cells, a better understanding of the physics involved in these materials is needed.

Photoluminescence (PL) is one of the most important optical methods for the characterization of semiconductor materials, with a particular relevance when they are intended for photonic applications such as solar cells. This technique probes the electronic structure of the semiconductor materials, revealing important information about the radiative and nonradiative recombination mechanisms. Recent works have shown PL characterization of different CZTS types of samples: bulk single crystals,[18,19] monograin powders,[20] and thin films prepared by sol-gel.[21] The optical transitions in chalcopyrite- and kesterite-type materials have been discussed regarding mainly the compositional dependencies and degree of doping. Different types of radiative transitions have been identified.[22] However, the PL emission is usually dominated by donor-acceptor pair (DAP) recombination or by transitions involving tail states in conduction and/or valence bands created by potential fluctuations.[19,22–25]

Electrical transport characterization is also one of the most used experimental techniques to study the electronic properties of semiconductor materials and devices. In particular, the analysis of the temperature dependence of the Hall effect and resistivity measurements provides valuable information about the electrical conduction mechanism in the samples as well as parameters such as charge-carrier concentration and mobility, which directly influence the performance of optoelectronic devices. The ionization energy and concentration of acceptor and donor centers as well as the compensation ratio in the samples are other parameters that can be accessed through these measurements. The information gathered by electrical transport characterization is essential to complement the data obtained by PL and to further understand the electronic structure of the samples and the physics of the recombination channels. In spite of the abundant reports on electrical characterization of ternary and quaternary chalcopyrite alloys

 ©2011 American Physical Society

related to CIGS,[22] no reports have been found for CZTS thin films similar to this one.

In this work, we discuss the PL observed for CZTS thin films grown through the sulfurization of metallic precursors deposited sequentially by direct current (dc) magnetron sputtering on a soda lime glass (SLG). The analysis of the PL properties, including excitation power and temperature dependencies of the broad PL band, enabled a comparison with existing models. Hall effect and electrical resistivity measurements as a function of temperature were also carried out to further understand the electronic structure of the samples and to support the interpretation of the PL emission. Our results are well described by the model of fluctuating potentials.

II. MATERIAL AND METHODS

The CZTS thin films were grown by sulfurization of metal precursors after their sequential deposition on SLG coated with and without molybdenum (Mo). The substrates were first cleaned with successive ultrasound baths of acetone/alchool/dionized water and dried with a N_2 flow. Then, for SLG coated with Mo, a Mo bilayer ($500 + 250$ nm, target purity of 99.95%) was deposited by dc magnetron sputtering to ensure both low resistivity and good adhesion to the SLG.[26] Following this step, the metallic precursors were deposited in an Ar atmosphere and at an operating pressure of 2×10^{-3} mbar according to the following order: Zn (target purity of 99.99%, thickness of the deposited layer: 260 nm), Cu (99.999%, 185 nm), Sn (99.99%, 300 nm). The deposition power settings were 0.16–0.38 $\mathrm{W\,cm^{-2}}$, 0.16 $\mathrm{W\,cm^{-2}}$, and 0.11–0.16 $\mathrm{W\,cm^{-2}}$ for Zn, Cu, and Sn, respectively. *In situ* monitoring of the layer thicknesses was done with a quartz crystal monitor. The sulfurization was done inside a tubular furnace in a nitrogen and sulfur atmosphere, and at an operating pressure of 5.6×10^{-1} mbar. The sulfur source was elemental sulfur pellets (purity of 99.999%). The details of the sulfur source and substrate temperatures profiles were discussed elsewhere.[7] The maximum temperature attained was 525 °C. After the sulfurization process, all samples studied in this work were submitted to a KCN chemical treatment to remove any $Cu_{2-x}S$ phases present.

The thicknesses of the individual metallic precursor layers and of the CZTS layer were measured with a Veeco Dektak 150 step profiler. The composition of the films was investigated by inductively coupled plasma mass spectroscopy (ICP-MS) using an ICP-MS Thermo X Series. Scanning electron microscopy (SEM) was used to investigate the morphology of the samples with a SEM Hitachi S4100 equipment. The structural characterization of the samples was carried out by X-ray diffraction (XRD) and micro-Raman spectroscopy (RS). XRD measurements were performed with a Philips PW 3710 diffractometer equipped with a Cu-K_α source ($\lambda = 1.540\,60$ Å). The RS spectra were recorded at room temperature using a Jobin Yvon T64000 triple spectrometer in the subtractive mode equipped with a charge-coupled detector. The 514.5 nm line of an Ar^+ laser was employed as an excitation source.

PL was performed in thin films grown on SLG coated with Mo with a continuous He flow cryostat, which allowed the change of temperature in the 5–300 K range. The 488 nm line of an Ar^+ laser was used as an excitation source and the emission from the samples was detected with a FTIR Bruker IFS 66v spectrometer equipped with a Ge detector cooled at liquid nitrogen temperature.

Electrical transport experiments were carried out to obtain additional information about the electronic structure of the samples and to support the interpretation of the PL data. Hall effect measurements were carried out in thin films grown on SLG without Mo, between 300 and 350 K under 0.7 T magnetic field in the Van der Pauw scheme. Au contacts were used with an active area of 24 $\mathrm{mm^2}$. Electrical conductivity measurements were done in a Van der Pauw configuration over the more extended, 16–350 K, temperature range.

III. RESULTS

In this work, we studied CZTS thin-film samples that resulted from a process of optimization of the growth parameters as described elsewhere.[7] The ICP-MS measurements revealed metallic ratios of $[\mathrm{Cu}]/([\mathrm{Zn}] + [\mathrm{Sn}]) = 0.9$ and $[\mathrm{Zn}]/[\mathrm{Sn}] = 1.3$, which show that the CZTS films are copper-poor and have a higher concentration of Zn than of Sn. These values are close to the composition of the films that showed the best solar cell efficiencies.[10,17]

The morphology of the grown films was investigated by SEM as shown in Fig. 1. The CZTS films show good crystallinity and compactness. The absence of faceted grains shows that the KCN treatment removed the $Cu_{2-x}S$ crystallites, as expected.

The structural evaluation of the CZTS thin films was done through XRD and RS measurements. In Fig. 2(a), we show the XRD diffractogram for a CZTS film. In addition to the three peaks related to the Mo layer, several reflections were observed. As discussed previously,[27] the latter peaks could be related either to CZTS or β-ZnS phases.[28] Their identification as reflections due to the CZTS phase comes after the comparison with the RS analysis [Fig. 2(b)] in which three CZTS-related peaks (287, 338, and 368 $\mathrm{cm^{-1}}$) (Refs. 20 and 27) are observed. The relative intensity of the shoulder at 348 $\mathrm{cm^{-1}}$ is very low, which suggests that the β-ZnS phase is not present in our films. In this way, the RS results allow us to conclude that the reflections observed in XRD are just due to the CZTS phase and that the films are single-phase.

From the XRD measurements, the values of $a = 5.424$ Å and $c = 10.861$ Å were obtained. Comparing these values with those for an unstrained film, $a = 5.435$ Å and $c = 10.843$ Å, relative shifts of 0.20% and 0.17% were found for a and c, respectively. This shows that the strain in the cell is negligible. Also, the obtained value of $c/2a = 1.001$ shows that the cell is tetragonal.

The electronic structure of the CZTS samples was investigated by PL spectroscopy. The low-temperature PL spectra of the CZTS thin films are shown for different values of excitation power in Fig. 3(a). The observed feature was an asymmetric broadband with a maximum of intensity at 1.24 ± 0.01 eV, which has an almost exponential increase in the low-energy side and is steeper in the high-energy side.

Figure 4 shows the dependence on the excitation power of the peak position and intensity. As the excitation power increases, the PL peak suffers a blueshift at a rate of 23.5 meV

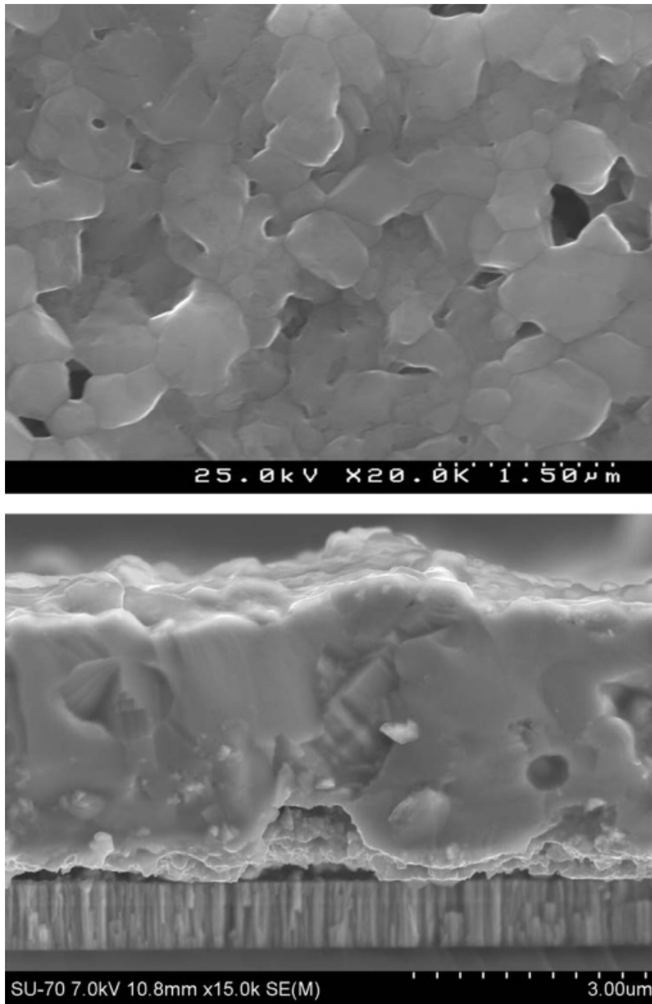

FIG. 1. SEM micrographs of the surface (top) and of a cross section (bottom) of a CZTS thin film grown by sulfurization of metal precursors after their sequential deposition on SLG coated with Mo. A KCN chemical treatment was applied to the films after the growth.

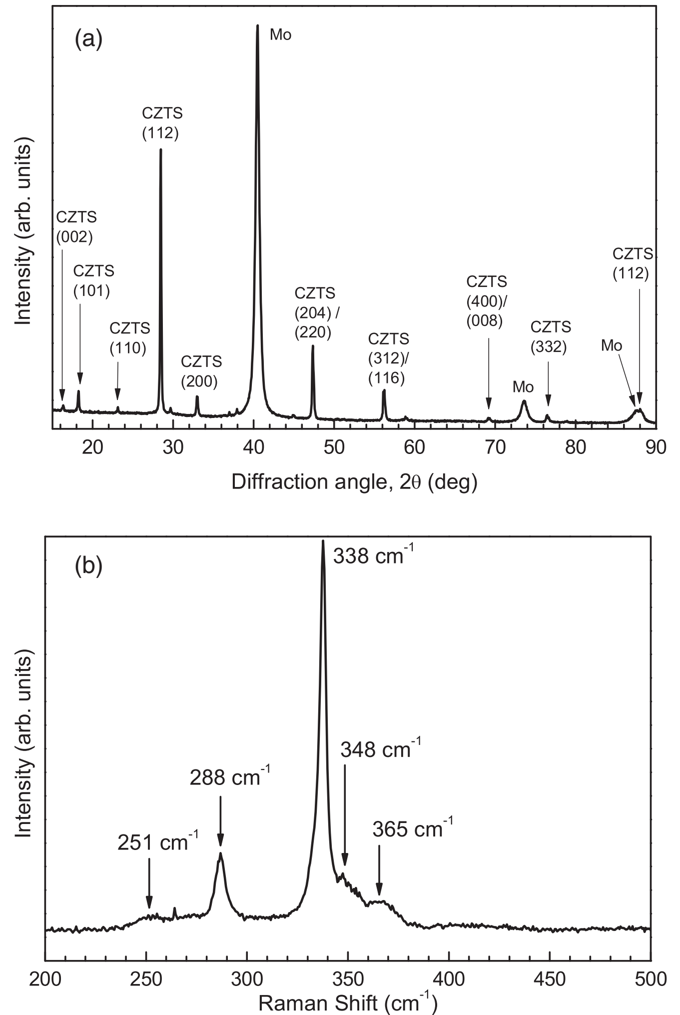

FIG. 2. XRD diffractogram (a) and Raman spectrum (b) obtained for a CZTS thin film grown over a Mo layer.

per decade. Additionally, the PL integrated intensity I follows the power law

$$I \propto P^m, \tag{1}$$

where P is the excitation power and m is an adjustable parameter. Values of $m < 1$ are typical of recombination mechanisms involving defects, while for $m > 1$ the transitions are excitonic.[29] From the fit of Eq. (1) to data in Fig. 4(b), a value of $m = 0.99 \pm 0.06$ was obtained.

To further investigate the recombination mechanism, PL emission was recorded as a function of sample temperature [Fig. 3(b)]. The increase of the temperature leads to the quenching of the PL intensity and a shift of the peak position to lower energies by ~ 24 meV in the range 5–160 K [Fig. 5(a)]. The dependence on temperature of the PL intensity is shown in the Arrhenius plot of Fig. 5(b), in which is visible a slow decrease for $T \lesssim 35$ K and a stronger one for higher temperatures.

Upon continuous photoexcitation, a steady-state density of free electrons and holes as well as free excitons is generated, which can be captured by the different types of defects present in our samples. As a consequence, these defects may be left in a radiative excited state. The intensity of the PL emission from these defects is strongly affected by the density of defects in radiative states and the temperature of the sample. As the temperature T is increased, the quenching of the PL intensity is observed as a consequence of the thermal activation of nonradiative channels for the escape of the charge carriers. These channels can involve discrete levels or a band. Different models for the description of the PL intensity quenching were considered, and the best fit to the data was obtained considering two nonradiative channels involving two discrete levels. These levels are separated from the radiative state involved in the PL emission by energies of E_1 and E_2, corresponding to the activation energies of the respective nonradiative channels. The dependence of the PL intensity on the temperature is given by[30]

$$I(T) = I_0(1 + c_1\, e^{-E_1/k_BT} + c_2\, e^{-E_2/k_BT})^{-1}, \tag{2}$$

where I_0 is the intensity extrapolated to $T = 0$ K and k_B is the Boltzmann constant. The above equation reflects the Maxwell-Boltzmann distribution of excitons and charge carriers between the radiative state and higher-energy levels. The parameters c_i $(i = 1,2)$ are proportional to the degeneracy

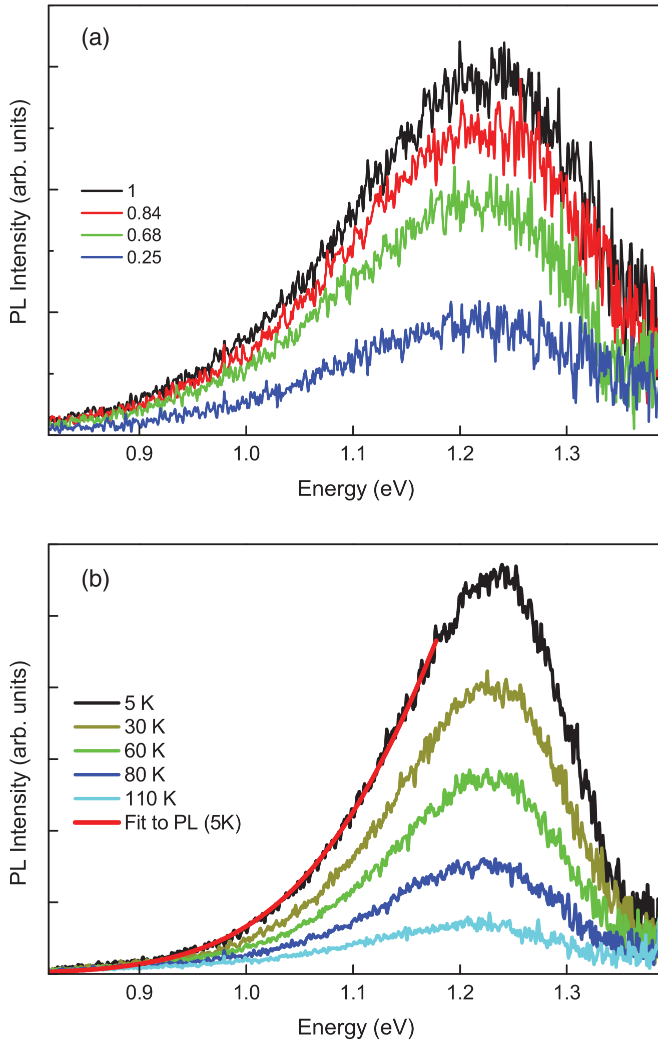

FIG. 3. (Color online) Photoluminescence of a CZTS thin film for different values of (a) excitation power; (b) temperature. The values of the excitation power were normalized to the maximum one. The excitation was done with the 488 nm line of an Ar^{+} laser. The PL intensity in the range 0.8–1.18 eV for the spectrum measured for 5 K (b) was fitted by Eq. (7).

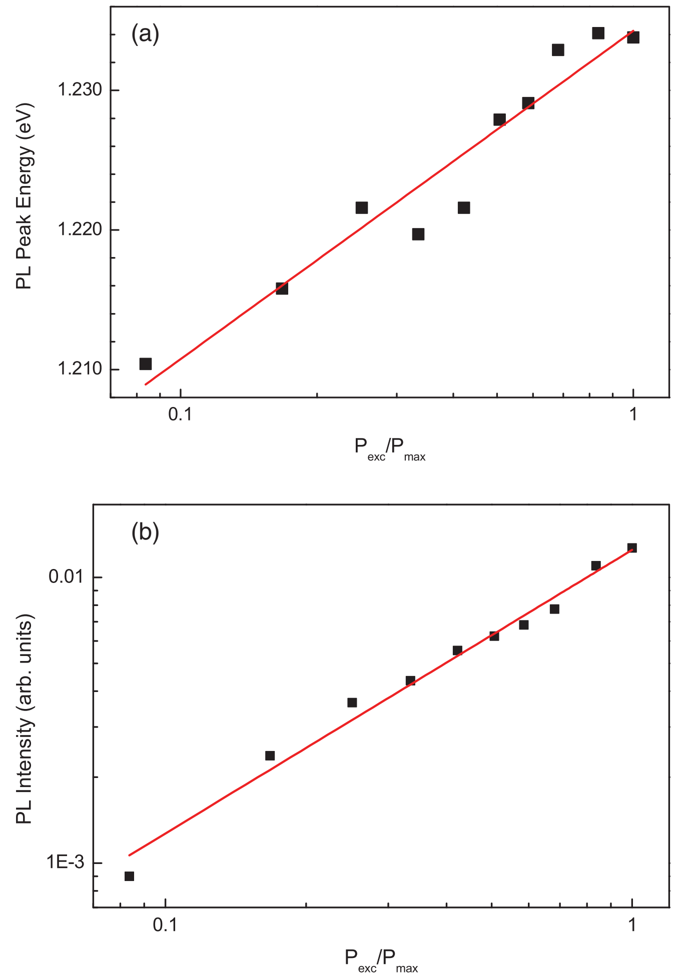

FIG. 4. (Color online) Dependence on the excitation power of (a) peak energy; (b) PL integrated intensity. The excitation was done with the 488 nm line of an Ar^{+} laser. The excitation power values were normalized to the maximum one. The data in (a) and (b) were fitted by a linear equation and by Eq. (1), respectively.

factor ratio between the corresponding level and the ground state. The fitting parameters are presented in Table I.

To have a full discussion of the radiative recombination mechanisms present in our samples, the PL results must be complemented with additional information about the physical parameters that characterize the presence of defects in our samples. As is well known from the literature,[22,31] the level and type of doping and the degree of compensation will determine the density of electronic levels inside the band gap and the eventual blurring of the energy-band edges. Depending on these properties, different types of radiative transitions have been discussed for chalcopyrite semiconductors.[22] Electrical measurements such as the Hall effect and electrical conductivity are well suited to give additional information needed to characterize the grown material. These experiments were carried out in different temperature ranges. For these measurements, we used samples in which the Mo bilayer was not deposited on top of the SLG. Otherwise, the Mo will create a parallel conduction channel hindering the analysis of the film. We must note that the crystalline phases for both samples gave similar results. No MoS_2 phase was observed for the samples grown with the Mo bilayer. While the electrical conductivity measurements were done in the 16–350 K range, Hall effect measurements were only possible in the 300–350 K range due to the very low Hall mobility of the carriers and their very high concentration. The Hall effect measurements have shown that the CZTS thin film presents a *p*-type conductivity, in agreement with hot point probe measurements.[7] Figure 6 shows the temperature dependence of the electrical conductivity, Hall concentration, and Hall mobility of the CZTS thin film.

Two types of conductivity mechanisms are usually observed in semiconductor samples. At high temperatures the conductivity can be described by free charge carriers. On the other hand, at low temperatures, the conductivity is explained in terms of hopping conduction associated with defects in the gap of the material. In Fig. 6, three temperature zones were observed: zone I, between 350 and 150 K, where free charge carriers dominate the conductivity; zone II, between

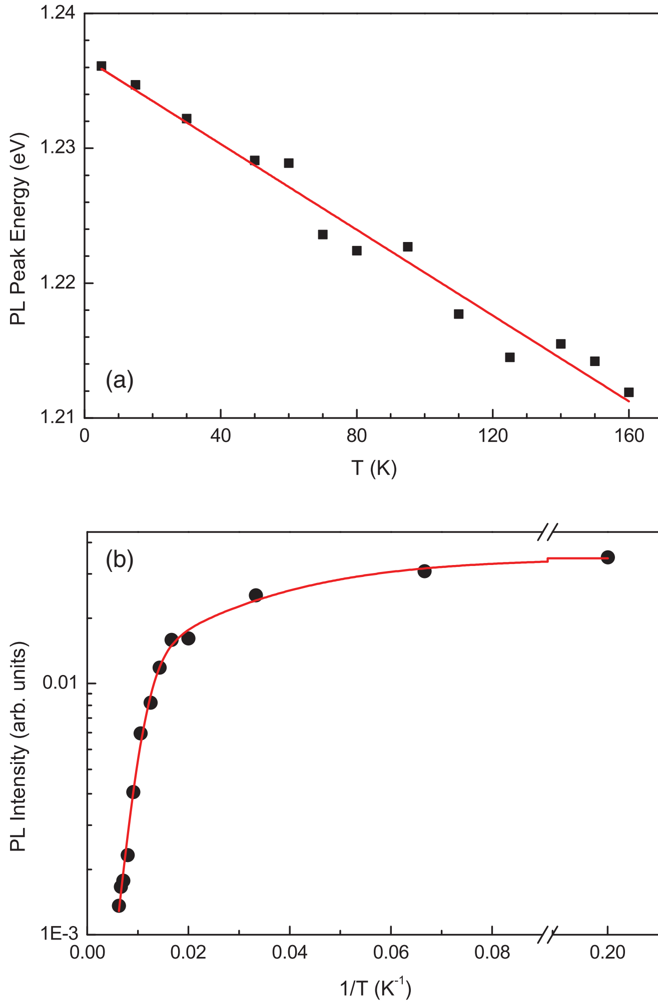

FIG. 5. (Color online) Dependence on the temperature of (a) peak energy; (b) PL integrated intensity. The excitation was done with the 488 nm line of an Ar^+ laser for an excitation power of 21 mW. The data in graphs (a) and (b) were fitted with a linear equation and Eq. (2), respectively.

150 and 50 K, where the above two mechanisms are involved; and zone III, for $T < 50$ K, where the conductivity is dominated by the hopping mechanism. To obtain values for the parameters relevant for the interpretation of PL data, such as the ionization energy of the acceptor level, the density of acceptors and donors, the degree of compensation, and free hole concentration, we will concentrate here on the analysis of the high-temperature zone.

At high temperatures, zone I, the electrical conductivity of polycrystals is dominated by the thermal emission of carriers over the intergrain potential barriers (GPB's). The temperature dependence of the electrical conductivity can then be expressed as[32]

$$\sigma(T) = e\,(\mu_0\, e^{-\phi/k_B T})\, p(T), \tag{3}$$

where e is the electron charge, μ_0 is a quantity with units of mobility and related to the average overall grain size in the sample, the exponential factor describes the thermal activation of the carrier mobility flowing over the GPB with height ϕ, and $p(T)$ is the temperature-dependent free hole concentration.

As shown in the inset of Fig. 6, the mobility of free holes is very low and almost independent of the temperature. Assuming no influence of the GPB in the high-temperature zone, the temperature dependence of the conductivity is then ruled by the temperature dependence of the free hole concentration in the bulk of the grains.

Considering that the sample is a nondegenerate semiconductor, as suggested by the strong temperature dependence of the conductivity data, and that the sample is p-type with a dominant acceptor and compensated by donors, the free hole concentration can be written as[33]

$$p(T) = \frac{1}{2}\left(\frac{g_{A_1}}{g_{A_0}} N_v^*\, e^{\alpha_A/k_B}\, T^{3/2}\, e^{-E_{A_0}/k_B T} + N_D\right) \times \left[\sqrt{1 + \frac{4\frac{g_{A_1}}{g_{A_0}} N_v^*\, e^{\alpha_A/k_B}\, T^{3/2}\, e^{-E_{A_0}/k_B T}(N_A - N_D)}{\left(\frac{g_{A_1}}{g_{A_0}} N_v^*\, e^{\alpha_A/k_B}\, T^{3/2}\, e^{-E_{A_0}/k_B T} + N_D\right)^2}} - 1\right], \tag{4}$$

where N_D is the concentration of ionized donors, N_A is the concentration of ionized acceptors, g_{A_0} and g_{A_1} are the degeneracy factors of the fundamental and first excited acceptor levels, respectively, $N_v^* = 2(2\pi m^* K_B)^{3/2}/h^3$, with m^* being the effective mass of the holes in the valence band, and $E_A(T) = E_{A_0} - \alpha_A T$ is the temperature dependence of the thermal ionization energy of the acceptor.

TABLE I. Fitting parameters of Eq. (2) to the dependence on temperature of the PL intensity.

I_0	c_1	E_1 (meV)	c_2	E_2 (meV)
0.0314 ± 0.0007	2.3 ± 0.5	4.1 ± 0.7	405 ± 261	40 ± 6

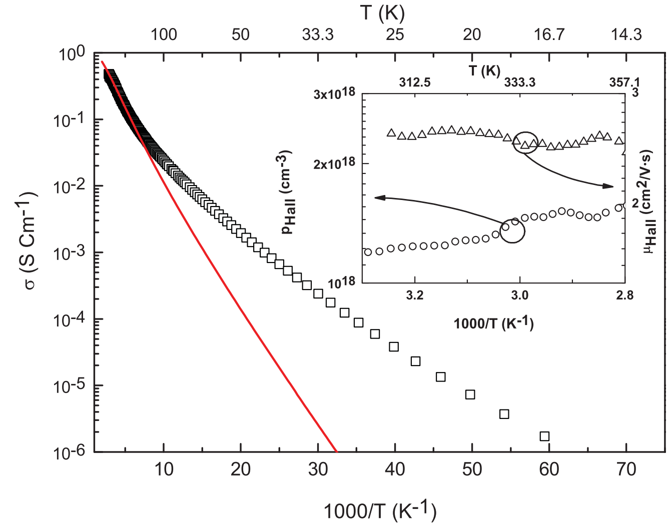

FIG. 6. (Color online) Temperature dependence of the electrical conductivity. The data on the high-temperature region were fitted with Eqs. (3) and (4). The Hall concentration and Hall mobility of the polycrystalline CZTS thin film in the 300 − 350 K region is shown in the inset.

Due to the narrow temperature range of the Hall effect measurements and the dispersion of the free hole concentration data (inset in Fig. 6), we extracted the relevant transport parameters by fitting the electrical conductivity data with Eqs. (3) and (4). The values of $N_A = 2.04 \times 10^{20}$ cm^{-3}, $K = N_D/N_A = 98\%$, $E_{A_0} = 29$ meV, and the prefactor $g_{A_0}/g_{A_1} N_v^* e^{\alpha_A/k_B} = 5.44 \times 10^{16}$ cm^{-3} K$^{-3/2}$ were obtained from the fit. From the obtained values, we see that the CZTS film is heavily doped and the degree of compensation is very high (98%).

The values obtained in this work for the Hall mobility are in the range 0.5–2 cm^2 V^{-1} s^{-1} and for the hole concentration around 10^{18} cm^{-3}. These values are close to those obtained by Tanaka *et al.*[34] for polycrystalline CZTS. In the case of CIGS,[35–37] and considering polycrystalline films for which the solar cells showed efficiencies close to the highest values reported, the mobilities are of a few cm^2 V^{-1} s^{-1}. However, the values for the hole concentration are approximately two orders of magnitude lower than the values reported in this work. This discrepancy shows that the control of the doping level in CZTS must increase.

IV. DISCUSSION

XRD, RS, and SEM measurements have shown that after the sulfurization of the precursors, only the CZTS phase was formed. Additionally, the KCN treatment successfully removed the $Cu_{2-x}S$ phases, as expected. The composition investigation by ICP-MS measurements revealed a metallic ratio that corresponds to a copper-poor CZTS thin film. In previous hot point probe measurements, a *p*-type conductivity has been observed for these samples.[7]

The emission observed in photoluminescence corresponds to an asymmetric broadband with a maximum of intensity at 1.236 eV and a full width at half maximum of ~ 0.17 eV, which differs from the assumed band-gap energy (~ 1.5 eV) for the undoped CZTS by ~ 0.26 eV. No other bands were observed in the spectral region under study. Broadbands with similar shape and peak positions in the same energy range have been observed by other authors.[18–21] To the best of our knowledge, this is the first time this emission has been observed in CZTS thin films prepared by sulfurization of metallic precursors.

In chalcopyrite– and kesterite–stannite-type semiconductors, different optical transitions involving excitons or charge carriers bound to levels introduced by defects have been observed.[19,22–25] Usually, the PL emission in these materials is dominated by radiative recombinations in donor-acceptor pairs (DAP's) or involving band-tail states created by fluctuating potentials. The appearance of each one of these types of radiative transitions depends mainly on the doping level of the semiconductor. For DAP transitions, the doping level is low, which results in point defects distributed randomly in the material.[38] The transitions involve charge carriers bound to donor and acceptor discrete levels in the band gap. When shallow donors and acceptors are involved, the characteristics of DAP transitions, for experiments in steady state, are a low coupling to the lattice, which allows the resolution of no-phonon and phonon-related bands, a moderate blueshift with the increase of the excitation power, and a blueshift with increasing temperature.[24,25] On the other hand, for highly doped and compensated semiconductors, the model of fluctuating potentials has been proposed.[31,39–41] In this model, tail states in conduction and/or valence bands appear as a consequence of potential fluctuations created by a large concentration of impurities, most of them charged. The average distance between impurities is lower than the Bohr radius of an impurity state and, as a consequence, the impurity levels suffer a broadening. The Coulomb potential created by each impurity is screened by free charge carriers. In the case of donors, the screening radius is given by

$$r_0 = \left(\frac{\pi}{3}\right)^{1/6} \left(\frac{a_e}{4\,n^{1/3}}\right)^{1/2}, \tag{5}$$

a_e being the Bohr radius of a donor state and n the density of free electrons. The density of states does not vanish at the edge of the respective band but forms tails in the band gap. The potential wells created by the above distribution of impurities can be characterized on average by r_0 and a root-mean-square depth γ which, for the case of the conduction band, is given by

$$\gamma = \sqrt{2\pi}\,\frac{e^2}{\epsilon\, r_0}\sqrt{N_d\, r_0^3}, \tag{6}$$

where ϵ is the dielectric permittivity of the semiconductor and N_d is the concentration of donors. The increase in the level of compensation will result in the lowering of the free-carrier density with a consequent increase of r_0 and γ.

Usually, for direct-band-gap semiconductors, the electrons have an effective mass much lower than the effective mass of the holes, $m_e \ll m_h$. In that case, the ground energy level of a hole is much deeper than for an electron in a similar potential well. This is due to the inverse proportionality between the energy of localization and the effective mass of the charge carrier ($\varepsilon_0 = \hbar^2/m^* r_0$). As a consequence, the density of states of the valence-band tail will have a much higher influence in PL. Recently,[42] an electron effective mass of $m_e \sim 0.18 m_0$ was calculated for CZTS, whereas for the hole effective mass a strong anisotropy was found. In any case, the hole effective mass should be higher than the electron effective mass.

In the case of strong compensation, heavily doped semiconductors may be nondegenerate.[41] Localized states associated with single acceptors with ionization energy E_I will be created in the band gap due to the large effective mass of holes. The broadening of these acceptor levels is parametrized by γ.

The optical pumping of the semiconductor will create nonequilibrium free electrons and holes that can recombine through different radiative and nonradiative channels. However, they will be predominantly captured in the tails in both bands or by the acceptor levels in the case of the holes. Several types of transitions have been discussed in the framework of the model of fluctuating potentials. The foreseen behavior under the change of temperature or excitation power is not uniquely dependent on the particular type of transition considered. In the case of nondegenerate heavily doped and strongly compensated semiconductors, the PL peak should shift to lower energies with the increase of temperature and

shift to higher energies with the increase of the excitation power.[41] Additionally, the intensity of the emission in the low-energy side of the broadband for the radiative recombination of an electron with a hole bound to an acceptor level is given by

$$I_{\mathrm{LE}}(h\nu) \propto \frac{1}{\gamma}\exp\left(-\frac{(E_g - E_I - h\nu)^2}{2\gamma^2}\right), \qquad (7)$$

where E_g is the band-gap energy of the doped semiconductor. This equation follows the density of states of the valence-band tail. E_g is related to the band gap of the undoped semiconductor, $E_g^0 = E_c^0 - E_v^0$, by[31]

$$E_g = E_g^0 - \gamma_e - \gamma_h - \Delta E, \qquad (8)$$

where $\gamma_e = E_c^0 - E_c$, $\gamma_h = E_v - E_v^0$ (E_c and E_v are the percolation levels), and ΔE describes the carrier density narrowing of the band gap. Equation (8) shows that the band-gap energy decreases with the doping level.

The obtained PL spectra (Fig. 3) show that the emission has approximately the same shape for all temperatures and excitation powers and no other bands were observed. This behavior suggests the same type of radiative transitions throughout the studied ranges of temperatures and excitation powers. The PL measurements have shown a peak shift to higher energies as the excitation power was increased [Fig. 4(a)] and a peak shift to lower energies with the increase of the temperature [Fig. 5(a)]. This experimental behavior is in contradiction to that observed for DAP-type transitions[24,25] but in accordance with the model discussed above.[41] A similar shift was observed in CIGS.[24]

The performed electrical conductivity measurements showed that the studied CZTS thin films are heavily doped and strongly compensated. The electrical conductivity data in Fig. 6 show a strong temperature dependence, which suggests a nondegenerate character of the films. Additionally, the free hole concentration shows an activation energy similar to the one observed in the electrical conductivity data ($E_a = 46$ meV) in the 300–350 K range. In this way, the electrical measurements support clearly the used model for the interpretation of the PL emission.

The increase of the temperature revealed a small decrease of the PL intensity for $T \lesssim 35$ K and a stronger quenching for higher temperatures [Fig. 5(b)]. This dependence was modeled by the thermal activation of nonradiative channels parametrized by the activation energies of $E_1 = 4.1 \pm 0.7$ meV and $E_2 = 40 \pm 6$ meV. The nonradiative channel for lower temperatures could be related to the release of electrons from shallow potential wells. This is compatible with the small depth of tails in the conduction band due to the small electron effective mass and with the nondegenerate character of the studied CZTS films. Alternatively, this channel could involve shallow energy levels introduced by other defects. The nonradiative channel for higher temperatures was attributed to the release of the holes from the acceptor levels to the valence band. The obtained value of $c_2 = 405 \pm 261$ suggests that the excited level involved in this mechanism has a much higher degeneracy factor than the radiative level. In this way, the ionization energy of the acceptor levels is 40 ± 6 meV. This ionization energy is also compatible with the activation energy obtained for the acceptor levels considered in the fitting of the electrical conductivity shown in Fig. 6.

Taking the spectrum obtained for 5 K in Fig. 3(b), we fitted with Eq. (7) the intensity of the emission in the range $0.80 < h\nu < 1.18$ eV. The obtained values for the parameters are $E_g - E_I = 1.412 \pm 0.008$ eV and $\gamma = 0.172 \pm 0.002$ eV. If we consider for E_I the value of the activation energy ($E_2 = 40 \pm 6$ meV) in the higher-temperature regime obtained from the temperature dependence of the PL intensity (Fig. 5), the estimated value for the band gap of the doped material is 1.452 ± 0.014 eV. The value for γ is high as expected for a strongly compensated semiconductor[31] and from the energy separation (~ 0.26 eV) of the PL peak with respect to the value of the band gap for the undoped material. Finally, the fact that the low-energy side of the emission reproduces the density of states of the valence-band tails shows that the distribution of impurities is correlated.[31]

The increase of the excitation power at low temperatures results in a shift of ~ 23.5 meV per decade to higher energies [Fig. 4(a)]. This value is clearly higher than the ones typically observed for transitions described by the DAP-type transitions.[24,25] This shift is in accordance with the type of radiative transitions proposed for the PL emission.[41] As shown in Fig. 4(b), the dependence on the excitation power of the PL intensity shows an exponent of $m = 0.99 \pm 0.06$. In heavily doped and strongly compensated semiconductors, the impurity levels are broadened, which will hinder the formation of excitons.[31] The intermediate value of m between the typical values for recombination mechanisms involving defects and excitons can be explained by the absence of the electron in a defect level.

We must recall that the composition evaluation gave a ratio $[\mathrm{Cu}]/([\mathrm{Zn}] + [\mathrm{Sn}]) = 0.9$. In Cu-poor CIGS[24] and $Cu_xGa_ySe_2$,[25] the reported optical transitions were also described by the model of fluctuating potentials, which supports the above interpretation of our results.

V. CONCLUSIONS

The sulfurization of metallic precursors gave rise to the formation of single-phase thin CZTS films with kesterite structure, grown on SLG substrates coated with and without Mo. A good crystallinity and compactness was found. The thin films were copper-poor and zinc-rich, close to the composition of the CZTS films in the solar cells with the best reported efficiency. Electrical conductivity measurements revealed heavily doped and highly compensated films. For the mobility of free holes, an almost independence on the temperature was found. The grown films showed a nondegenerate character. A broad and asymmetric band, with peak energy at 1.24 ± 0.01 eV, was observed in PL measurements, which shifted to higher energies with the increase of excitation power and to lower energies as the temperature was increased. A model of radiative recombination of an electron with a hole bound to an acceptor level with a broadening parametrized by a fluctuation γ was proposed. The ionization energy of the acceptor level was estimated in the range 29–40 meV, whereas a value of 172 ± 2 meV was obtained for the potential fluctuation in the valence-band edge.

ACKNOWLEDGMENTS

P.A.F. and P.M.P.S. acknowledge the financial support of the Fundação para a Ciência e Tecnologia (FCT), through the PhD Grants No. SFRH/BD /49220/2008 and No. SFRH/BD/29881/2006, respectively. The authors acknowledge the FCT/CAPES joint project "Novos materiais para células fotovoltaicas: Calcopirites, kesterites e nanoestruturas de semicondutores III-V." FCT is also acknowledged for the financial support of the national electronic microscopy network (Grant No. REDE/1509/RME/2005).

*joaquim.leitao@ua.pt

[1] M. A. Green, Physica E **14**, 65 (2002).
[2] P. Jackson, D. Hariskos, E. Lotter, S. Paetel, R. Wuerz, R. Menner, W. Wischmann, and M. Powalla, New world record efficiency for Cu(In,Ga)Se2 thin-film solar cells beyond 20%, Progress in Photovoltaics: Research and Applications.
[3] H. Katagiri, N. Sasaguchi, S. Hando, S. Hoshino, J. Ohashi, and T. Yokota, Sol. Energy Mater. Sol. Cells **49**, 407 (1997).
[4] J. S. Seol, S. Y. Lee, J. C. Lee, H. D. Nam, and K. H. Kim, Sol. Energy Mater. Sol. Cells **75**, 155 (2003).
[5] K. Tanaka, N. Moritake, and H. Uchiki, Sol. Energy Mater. Sol. Cells **91**, 1199 (2007).
[6] S. Chen, X. G. Gong, A. Walsh, and S.-H. Wei, Appl. Phys. Lett. **94**, 041903 (2009).
[7] P. A. Fernandes, P. M. P. Salomé, and A. F. da Cunha, Semicond. Sci. Technol. **24**, 105013 (2009).
[8] J. P. Leitão, N. M. Santos, P. A. Fernandes, P. M. P. Salomé, A. F. da Cunha, J. C. González, and F. M. Matinaga, Thin Solid Films.
[9] H. Katagiri, K. Saitoh, T. Washio, H. Shinohara, T. Kurumadani, and S. Miyajima, Sol. Energy Mater. Sol. Cells **65**, 141 (2001).
[10] H. Katagiri, Thin Solid Films **480–481**, 426 (2005).
[11] K. Jimbo, R. Kimura, T. Kamimura, S. Yamada, W. S. Maw, H. Araki, K. Oishi, and H. Katagiri, Thin Solid Films **515**, 5997 (2007).
[12] N. Nakayama and H. Ito, Appl. Surf. Sci. **92**, 171 (1996).
[13] N. Kamoun, H. Bouzouita, and B. Rezig, Thin Solid Films **515**, 5949 (2007).
[14] M. Y. Yeh, C. C. Lee, and D. S. Wuu, J. Sol-Gel Sci. Technol. **52**, 65 (2009).
[15] T. M. Friedlmeier, H. Dittrich, and H. W. Schock, *in Ternary and Multinary Compounds, proceedings of the 11th International Conference on Ternary and Multinary Compounds, Salford, 1997,* edited by R. D. Tomlinson, A. E. Hill, and R. D. Pilkington (Institute of Physics Pub., Bristol, 1998), p. 345.
[16] K. Wang, O. Gunawan, T. Todorov, B. Shin, S. J. Chey, N. A. Bojarczuk, D. Mitzi, and S. Guha, Appl. Phys. Lett. **97**, 143508 (2010).
[17] T. K. Todorov, K. B. Reuter, and D. B. Mitzi, Adv. Mater. **22**, E156 (2010).
[18] K. Tanaka, Y. Miyamoto, H. Uchiki, K. Nakazawa, and H. Araki, Phys. Status Solidi A **203**, 2891 (2006).
[19] K. Hönes, E. Zscherpel, J. Scragg, and S. Siebentritt, Physica B **404**, 4949 (2009).
[20] M. Altosaar, J. Raudoja, K. Timmo, M. Danilson, M. Grossberg, J. Krustok, and E. Mellikov, Phys. Status Solidi A **205**, 167 (2008).
[21] Y. Miyamoto, K. Tanaka, M. Oonuki, N. Moritake, and H. Uchiki, Jpn. J. Appl. Phys. **47**, 596 (2008).
[22] S. Siebentritt, in *Wide Gap Chalcopyrites*, Springer Series in Materials Science, edited by S. Siebentritt and U. Rau (Springer, New York, 2006), pp. 113–156.
[23] P. W. Yu, J. Appl. Phys. **47**, 677 (1976).
[24] I. Dirnstorfer, Mt. Wagner, D. M. Hofmann, M. D. Lampert, F. Karg, and B. K. Meyer, Phys. Status Solidi A **168**, 163 (1998).
[25] A. Bauknecht, S. Siebentritt, J. Albert, and M. Ch. Lux-Steiner, J. Appl. Phys. **89**, 4391 (2001).
[26] J. H. Scofield, A. Dude, A. Albin, B. L. Ballard, and P. K. Predecki, Thin Solid Films **260**, 26 (1995).
[27] P. A. Fernandes, P. M. P. Salomé, and A. F. da Cunha, Thin Solid Films **517**, 2519 (2009).
[28] International Centre for Diffraction Data, 14 04-005-0388 (CZTS), 04-004-3804 (Cubic-ZnS), 04-004-3831 (Orthorhombic-Sns), 04-003-4154 (Hexagonal-SnS2), 04-001-1461 (Hexagonal-CuS).
[29] T. Schmidt, K. Lischka, and W. Zulehner, Phys. Rev. B **45**, 8989 (1992).
[30] G. Davies, Phys. Rep. **176**, 83 (1989).
[31] A. P. Levanyuk and V. V. Osipov, Sov. Phys. Usp. **24**, 187 (1981).
[32] J. W. Orton and M. J. Powell, Rep. Prog. Phys. **43**, 81 (1980).
[33] D. C. Look, *Electrical Characterization of GaAs Materials and Devices* (Wiley, New York, 1989).
[34] T. Tanaka, T. Nagatomo, D. Kawasaki, M. Nishio, Q. Guo, A. Wakahara, A. Yoshida, and H. Ogawa, J. Phys. Chem. Solids **66**, 1978 (2005).
[35] Th. Meyer, F. Engelhardt, J. Parisi, and U. Rau, J. Appl. Phys. **91**, 5093 (2002).
[36] S. Ishizuka, H. Shibata, A. Yamada, P. Fons, K. Sakurai, K. Matsubara, and S. Niki, Appl. Phys. Lett. **91**, 041902 (2007).
[37] S. A. Dinca, E. A. Schiff, B. Egaas, R. Noufi, D. L. Young, and W. N. Shafarman, Phys. Rev. B **80**, 235201 (2009).
[38] J. J. Hopfield, D. G. Thomas, and M. Gershenzon, Phys. Rev. Lett. **10**, 162 (1963).
[39] B. I. Shklovskii and A. L. Efros, *Electronic Properties of Doped Semiconductors* (Springer, Berlin, 1984).
[40] A. P. Levanyuk and V. V. Osipov, Sov. Phys. Semicond. **7**, 721 (1973).
[41] A. P. Levanyuk and V. V. Osipov, Sov. Phys. Semicond. **7**, 727 (1973).
[42] C. Persson, J. Appl. Phys. **107**, 053710 (2010).